sustainability

MDPI

Article

Experimental Investigation of Mass Transfer Intensification for CO_2 Capture by Environment-Friendly Water Based Nanofluid Solvents in a Rotating Packed Bed

Farhad Ghadyanlou [1], Ahmad Azari [1,*] and Ali Vatani [2]

[1] Faculty of Petroleum, Gas and Petrochemical Engineering (FPGPE), Persian Gulf University, Bushehr 75169-13817, Iran; ghadyanlou@mehr.pgu.ac.ir
[2] School of Chemical Engineering and Institute of LNG, College of Engineering, University of Tehran, Tehran 14179-35840, Iran; avatani@ut.ac.ir
* Correspondence: azari.ahmad@gmail.com or azari.ahmad@pgu.ac.ir; Tel.: +98-9173238639; Fax: +98-7733445182

Abstract: In this research, two intensification approaches for CO_2 capture via a rotating packed bed (RPB) and nanofluids were examined simultaneously to maximize the experimental mass transfer coefficient. The two intensification approaches were done by using water as a green, environmentally friendly absorption solvent and as the base fluid for preparing nanofluids and also by using centrifugal acceleration in an RPB. Physicosorption of CO_2 in an RPB was carried out by applying Al_2O_3, TiO_2, and SiO_2 nanofluids to intensify the mass transfer in water, and the operation parameters such as the angular speed of the rotor, concentration and type of nanoparticles, gas and liquid flow rates, and CO_2 concentration in mass transfer intensification were evaluated and several nanofluids were selected to survey investigate how they affect the mass transfer at low pressure. The results show that the Al_2O_3 nanofluid was more effective than other nanofluids and that the 40 nm nanofluid of this type was more efficient than the 20 nm size. Therefore, a correlation is proposed in this paper for liquid volumetric mass transfer coefficient prediction that includes the microconvection of nanoparticles and surface tension.

Keywords: RPB; CO_2 capture; nanofluids; mass transfer coefficients; nanoparticles; Weber number

Citation: Ghadyanlou, F.; Azari, A.; Vatani, A. Experimental Investigation of Mass Transfer Intensification for CO_2 Capture by Environment-Friendly Water Based Nanofluid Solvents in a Rotating Packed Bed. *Sustainability* **2022**, *14*, 6559. https://doi.org/10.3390/su14116559

Academic Editors: Steliana Rodino, Marian Butu and Alina Butu

Received: 21 April 2022
Accepted: 24 May 2022
Published: 27 May 2022

1. Introduction

It is well known that the main energy generation sources are still gas, oil, and fossil fuels all over the world. Pollution has led to global warming, melting ice in the South and North poles, the rising of sea and ocean levels, and climate change. Therefore, researchers are increasingly focusing on finding appropriate and optimal methods for gas treatment, especially carbon dioxide emissions [1].

There are four approaches to reducing gaseous emissions, namely, electrochemical, oxy-fuel combustion, pre-combustion, and post-combustion methods [2]. Carbon dioxide is mostly a greenhouse gas that plays a major role in climate change and is often absorbed in post-combustion processes in industries. These processes and other relevant technologies are developed to increase efficiency and decrease costs. Absorption and chemisorption are especially important in industries [2–4]. A good patent review on CO_2 removal technologies can be found in [5]. All technologies have their own advantages and disadvantages when used alone; therefore, to reduce the drawbacks, several intensification approaches are simultaneously applied. Song et al. called these "hybrid processes" [6]. Other techniques include the formulation of solvents [7,8] and process intensification tools such as centrifugal, vibration, mixing, nanoparticle, and magnetic field applications [9,10]. Process intensification (PI) helps to reduce equipment size, energy consumption, and effluents. and allows the systems to be compacted in smaller areas with innovations [11–13]. Rotating

packed beds (RPBs) are a type of PI equipment that uses centrifugal acceleration [14]. Another alternative PI approach, which was mentioned above, is the use of nanofluids (NFs) that include the suspension of nanoparticles (almost less than 100 nm) in a base fluid (BF) that can transfer heat and improve MT operations such as liquid-liquid extraction [15]. A great number of investigators have worked on CO_2 capture by using NFs, and a short review of these studies was published by Zhang et al. [16]. Previous investigation reports illustrated that Al_2O_3, TiO_2, and SiO_2 NFs are most effective MeOH-based NFs in CO_2 absorption. For instance, Pineda et al. [17] examined the enhancement of Al_2O_3 and SiO_2 and demonstrated that CO_2 absorption increased by more than 9% with these NFs. Lee and Kang [18] evaluated CO_2 solubility with Al_2O_3/NaCl aqueous NFs and reported 12.5% intensifiction. Jiang et al. [19] studied amine-based NFs and showed that TiO_2 and Al_2O_3 were more efficient than SiO_2. Haghtalab et al. [20] studied water-based ZnO and SiO_2 NFs in concentrations of 0.05, 0.1, 0.5, and 1 wt.% and compared the amounts of their enhancement at high pressures. Similarly, Al_2O_3 was examined in a concentration range of 0–0.2 wt.% in pure water and the optimum concentration value of 0.05% wt was reported In the results by Ref. [21]. Another example is the examination in mass fractions of 0.02, 0.1, 0.5, and 1% of Al_2O_3, SiO_2, Fe_3O_4, and CNT NPs in water and amine solution by Rahmatmand et al. [22], who reported that Al_2O_3 and SiO_2 were more efficent NFs. Darvanjooghi et al. [23] evaluated an SiO_2 NF with different sizes at concentrations of 0.005, 0.05, 0.01, and 0.1 and the results indicated that maximum CO_2 removal occured at the concentration of 0.01 wt.% and that the rate of absorption increased with the increase in NP size.

Salami and Salimi [24] used water-based NFs to enhance the MT rate in packed bed columns and reported that Al_2O_3 and SiO_2 NFs with a nanoparticle (NP) concentration of 0.05 vol.% had MT rates of 14% and 10%, respectively. In addition, some researchers, such as Samadi et al. [25] and Salimi et al. [26], applied magnetic NFs and magnetic field induction to achieve higher MT rates. These types of NFs enjoy two benefits: They are controllable in magnetic fields and help with CO_2 capture [27]. The simple or single-block RPB includes a liquid distributor and a rotor made up of a packing and a shaft. It should be noted that the liquid acceleration is set based on the rotor speed, which can intensify micro-mixing and MT according to its pattern. The change in the flow area is more significant in RPBs than in PBCs; therefore, the MT coefficient varies at different points of the rotor because of gas velocity and surface area changes along the radius [28]. It is clear that RPBs have a larger surface area than conventional PBCs in the same operation conditions [10]. Wang et al. [29] reported that advantages of RPBs were high volumetric MT coefficients (leading to a decreased physical size, as well as lower capital and operation costs), decreased flooding tendency, micro-mixing improvement, suitability for toxic and expensive materials, and skied-mounted applicability. Recently, Luo et al. [30] studied micro-mixing by applying two intensification approaches (ultrasonic-assisted RPB), and Dashti and Abolhasani [31] examined physicochemical absorption using MEA and NPs with TiO_2/MEA (0.01–0.1 wt.%) in an RPB with blade packing. They used TiO_2 based on the results of [19] and reported precipitation of particles not possible in RPBs because of high interactions and very low resistant time of the NFs.

Because of the advantages, RPBs are still designed and developed on laboratory and industrial scales. Generally, this topic is treated and developed in four directions:

(a) Examination of chemical solvents like propylene carbonate to evaluate the absorption ability [32]; mixed-chemical solvents, as in Ref. [33]; or new advanced-green solvent performance in acid gas treatment, such as ionic liquids [34] and nanofluids [31].

(b) Optimization of RPB operations by improving contact surface area or mass transfer by changing the hydrodynamic features through:

- Modifications to RPB configurations such as "liquid distributor(s)." For instance, Hacking et al. [35,36] examined novel redistribution rings in a bed. Wu et al. used a multi-inlet to distribute liquid in a bed [37] whose efficiency was examined by Zhang et al. [38], and Wang et al. [39] evaluated the contacting angle of fluids,

- Modifications to the bulk zone by adding baffles/blades, as in Yang et al. [40], or mesh pin, as in Liu et al. [41,42]; or changing the number of mesh screen layers, as in Su et al. [43]; changing the packing wettability, as Lu et al. [44]; or changing the kind of packing structure, as reported in [45].

(c) Examination of the intensification by replacing the conventional equipment with RPBs, such as deoxygenation of water and fuel [46,47], wastewater treatment [48], CO_2 absorption [49], and selective absorption [50].

(d) Focusing on the micro-scale or micro-mixing in a heat-sensible process, controlling polymerization processes, and packing optimization [51].

All of these development were carried out by experimental methods (tests or high-speed photography), CFD (reviewed by Chen et al. [52]), and numerical methods, especially the artificial neural network (ANN) method [53,54].

Regarding the first category, numerous CO_2 absorption systems in RPBs have been investigated by researchers at different operating parameters. Jiao et al. [55] examined the performance of an RPB in a Q_L range of 0.5–1 L/min and a Q_G range of 667–1667 L/min at 1 bar and 298 K. Generally, Xing et al. [56] showed RPB performance at atmospheric pressure in different rotational speeds and a vast gas–liquid ratio (GLR) range of more than 20 and up to 20,000, as summarized in Table 1. In addition, Xiang et al. [32] evaluated CO_2 absorption with propylene carbonate in a pilot-scale RPB at a gas flow rate of 8–25 m^3/h and liquid flow rate of 100–300 L/h at high pressure and a rotating speed of 290–1450 rpm.

Table 1. Temperature and GLR range selected for the CO_2 absorption system by previous investigators.

Authors	Temp., K	GLR
Wang et al. [33]	298–333	100–260
Lin et al. [57]	301	20–350
Yu et al. [58]	313–323	300–1200
Kang et al. [59]	333	67–700
Sheng et al. [60]	303–333	72–700
Wu et al. [61]	323	75–300
Sheng et al. [62]	303–323	138–242

The higher possible GLR for CO_2 absorption in an RPB is an important parameter to provide economical performance, as reported in [63], which allows operation with the lowest absorption solvent solution.

Considering the above issues, the present study focused on physical absorption and was carried out with two intensification approaches by an RPB as a contactor that provided centrifugal force and NPs that were applied to increase the effectiveness of water-based NFs as advanced environmentally friendly water-based solvents. Therefore, this study examined the effect of NFs on the MT coefficients at low pressure and CO_2 concentrations in a centrifugal field in an RPB. In this device, the cavity zone was removed with a modification of the contactor and was filled by packing to extend the gas–liquid contact area. Injections were mounted on the shaft and the liquid was distributed through the holes on the rotor, which could cool down the bearings in operation. On the other hand, we applied TiO_2, Al_2O_3, and SiO_2 nanoparticles in CO_2 capture. In this article, first, the setup characteristics, operation, and data processing of CO_2 capture by NFs are described, and then the results are evaluated and discussed.

2. Experimental Setup and Data Processing

2.1. Materials and Solvent Preparation

NPs (>99% purity) with the physical properties listed in Table 2 were purchased from different companies: Al_2O_3 (40 nm) from Neutrino Nanotechnology, TiO_2 (25 nm)

from Evonik Degussa Gmbh (Essen, Germany), and SiO_2 (5 nm) and Al_2O_3 (20 nm) from US Nano (South Bend, IN, USA). These NPs were applied to prepare water-based NFs (suspension) by adding NPs in pure water (DW) to produce 0.05–0.1 wt.% NFs as solvents after mixing by a magnetic stirrer. Ultrasonication of the water suspension was carried out using a probe-type device (UW-3100, Bandelin, Germany). It should be mentioned that water was selected to create an environmentally friendly BF. Then, the water–based NF was used as a solvent without adding any surfactant, but the stability of the NFs was examined by dynamic light scattering (DLS) analysis. The results are shown in Figure 1.

Table 2. Physical properties of the nanoparticles and BF applied in this study.

Solvent / Parameter	Base Fluid	Silica	Titanium Oxide	Alumina	
Color	Colorless	White	White	White	
Formula	H_2O	SiO_2	TiO_2	Al_2O_3 (I)	Al_2O_3 (II)
Density, Kg/m^3	998.2	2400	3800	3890	3920
Thermal conductivity, W/m.K	0.61	1.4	11.7	30	30
Molecular weight, g/mol	18.02	60.08	79.87	159.69	
Mean size of particles (nm)	—	3–10	25	20	40
Status or morphology	liquid	Spherical solid powder			
Purity	DM	>99.9%			
C_p (J/Kg.K)	4182	730	689.3	840	880
Surface tension (mN/m)	72.03	52	67.4	57.4	68.9

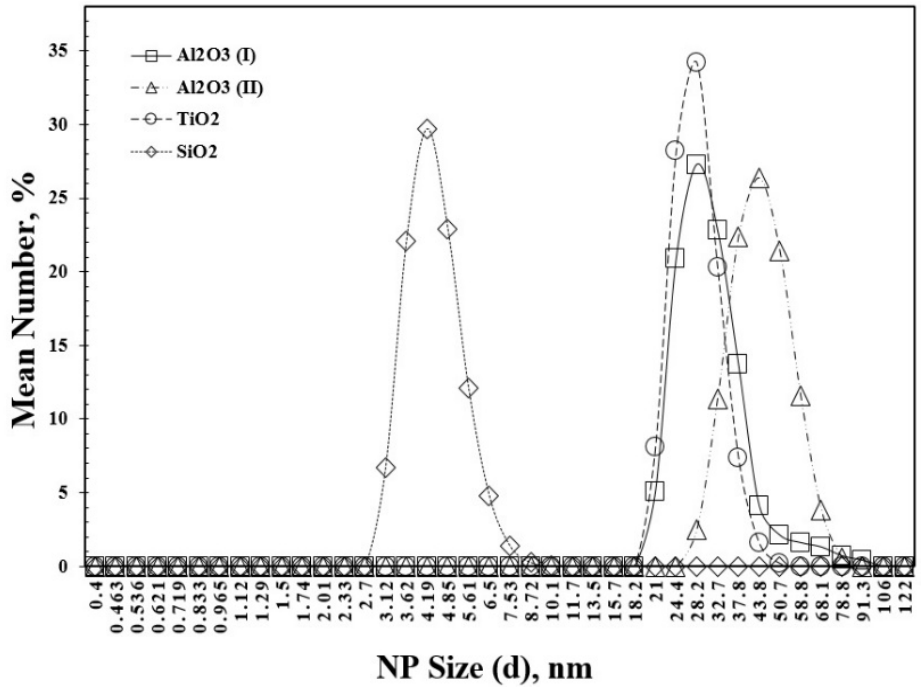

Figure 1. DLS analysis of NFs by number.

Investigation was performed after every 5 test runs and the NFs were sonicated again to make sure that they were dispersed well, although the turbulences of the fluid in the RPBs help the stability of the suspension, as reported by Dashti and Abolhasani [31].

2.2. Setup Characteristics, Operating, Data Gathering, and Processing

The novel RPB included a rotor that consisted of stainless-steel packing and small holes mounted on the shaft as liquid injectors, which were expected to help distribution. The cavity zone was filled by packing to increase the contacting area in the rotor. NFs as

solvents were injected with a nozzle into the center of the shaft and radially distributed in the packing to help cool the bearings. A gas stream was inserted circumferentially from the side of the casing (shell) into the center of the packing, made contact with the liquid droplets, and then left from via the housing.

As shown in Figure 2a, the setup used for CO_2 capture included an RPB, an electromotor, a pump, a vessel of NFs, tubes, connections, pressure gauges, flow meters, and cylinders of CO_2 and N_2. The regeneration section of [64] was used in this study to generate the CO_2-enriched stream.

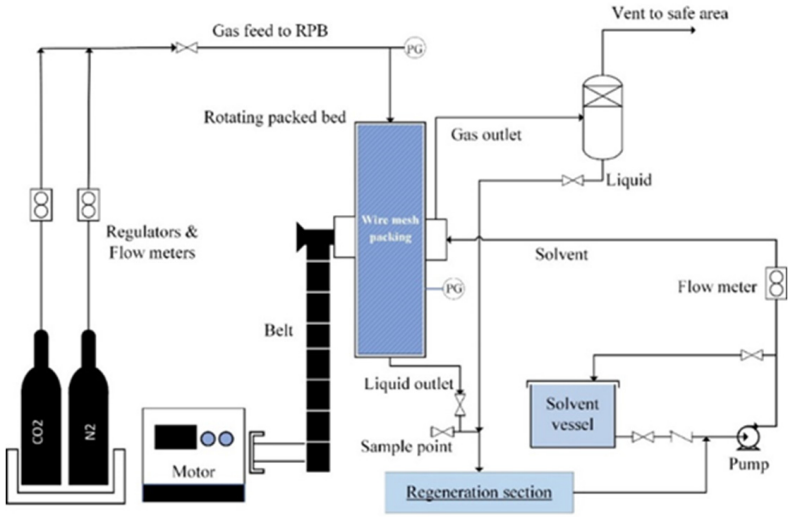

(**a**)

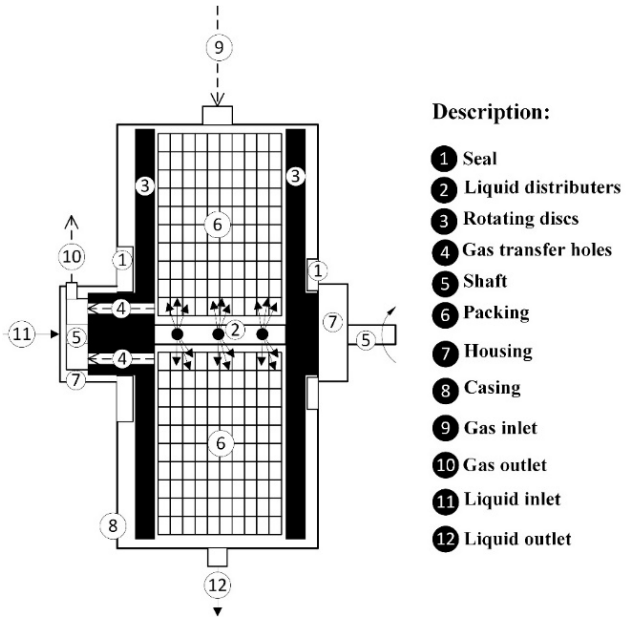

(**b**)

Figure 2. (**a**) Schematic of the experimental setup arrangement, (**b**) detail of the RPB.

After a leak test of the setup, test runs were performed by introducing gas from the top outside edge of the RPB casing, as shown in Figure 2b, which, after passing through the packing, exited the left housing from outlet gas holes. Simultaneously, the NF was injected into the rotor and distributed radially from small holes that were mounted on the shaft to

make contact with the gas stream counter-currently. The gas outlet stream was sent to a safe location, and the liquid outlet was sent to the regeneration section. After the solvent was regenerated, it was recycled to the NF storage vessel. The sampling point for titration was at beginning of the liquid stream towards to the regeneration section.

The experiment steps for NFs included:

1. Introducing the mixed gas stream to the RPB under a flow control and design limitation of system, then venting it out to a safe location.
2. Turning on the RPB driver at low speed and checking the operating condition.
3. Turning on the solution pump, introducing the solvent to the RPB slowly, setting the operating conditions with the instrument devices, and keeping the proper situation (Table 3).
4. Starting the regeneration section and recycling the regenerated solution stream to the solution pump suction when a steady-state situation is reached, then closing the outlet of the solvent vessel and keeping the circulation circuit.
5. At this stage, the rotating speed can be changed when stability of the system is reached.
6. Sampling for titration is caried out after 10 min.

Table 3. Rotating packed bed specifications and conditions of the experimental runs.

Packing Type	Stacked Layers of Wire Mesh
Inner diameter of rotor (shaft diameter), m	0.035
Outer diameter of rotor (disc diameter), m	0.255
Packing height, m	0.034
Total surface area (m^2. m^{-3})	563.04
Surface tension of packing, mN/m	75
Porosity	0.8958
Rotational speed (rpm)	300 & 500
Liquid flow rate, L/hr	24–42
Gas flow rate, L/min	6–16
CO_2 present range, %	10–50
Temperature, °C	35
Casing pressure, bar	3.3

According to Section 1, CO_2 absorption was performed by NFs in the operating conditions given in Table 3—that is, above atmospheric pressure while considering the design condition of the RPB.

The RPB with stainless steel wire mesh packing shown in Figure 2b, which was used in this research, had a packing with a 0.0175, 0.1275, and 0.034 m inner radius, outer radius, and axial height, respectively.

The uncertainty errors of experimenting instruments and the maximum errors of parameters are given in Tables 4 and 5, respectively.

2.3. Experimental Mass Transfer Modeling and Analysis

It should be noted that the mean MT coefficient is meaningful when the hydrodynamic condition is uniform throughout the whole system [65] and that there is no such unifurmity in an RPB. Moreover, theoretical and empirical approaches can be used for computing MT coefficients for simple systems, but there is no general theory to predict MT coefficients in RPBs [66]. Therefore, researchers present a suitable MT correlation for their system. Various empirical and statistical correlations for RPB contactors were developed and a greater number of effective parameters were considered by numerous researchers for many systems with several configurations of RPBs to raise the accuracy, as reported in [67]. For instance, Chen et al. studied RPBs with different radius values and reported that MT decreased with the increase in the outer radius of the packing at low rotational speeds, but this decrease was very low at high rotational speeds [68]. Later, they carried out a new investigation to evaluate MT in RPBs by considering the effect of packing characteristics such as size, material shape, and surface property, and they proposed a correlation that

included packing characteristics and fluid surface tension [69]. Rajan et al. [70] reported that k_La_e and a_e changed with several radius values of RPB (with ring packings) due to gas and liquid superficial velocity variations with centrifugal acceleration, which could affect the *Re* and *Fr* numbers. In addition, they reported that the Weber number (*We*) would be changed with the packing surface area. Mohammaddoost et al. [64] also examined physical absorption with metal oxides and developed correlations that were illustrated by [71,72] and showed that the Sherwood number (*Sh)* depended on the geometry of the contactor, liquid Schmidt number (*Sc*), NP volume fraction, liquid, and NP Reynolds number.

Table 4. Uncertainty of the instruments.

Instrument Name	Instrument Range	Measured Variable	Accuracy	Min and Max Values Measured in Experiment	Uncertainty (U%)
Gas flow meter	0–20 L/min	Volume flow rate of gas	0.1 L/min	6–16 L/min	0.01–0.03
Liquid flow meter	0–200 L/h	Volume flow rate of liquid	0.6 L/h	24–42 L/h	0.99–2.32
Titration glassware	0–50 ml	Volume of liquid	0.1 mL	0–30 ml	0.15–10
Thermometer	−200–850 °C	Inlet and casing temperatures	0.1 °C	30–35 °C	0.44
Scale	0–300 g	Weight of NPs	0.0001 g	0.025–0.25 g	0.05–0.15

Table 5. Uncertainty of the parameters.

Variable	Uncertainty Error (U%)
k_La	6.82
Re_L	0.89
Re_G	0.96
We	1.04
Gr	1.56
Sc	0.08
$k_La d_p/D_L.a_t$	1.36
Re_{NP}	1.10

In an RPB, the whole specific or total surface area (a_t), that is available with packing is not involved in MT. The specific surface area of packing is divided into wetted surface area (a_w) and gas–liquid MT effective interfacial surface area (a_e) due to the situation of the contacting phases in gas–liquid systems. All the wetted surface area in the vicinity of the gas phase generates the MT interface, and this determines the main value of the gas–liquid effective interfacial surface area. The dynamic status of hydrodynamics and their variation through an RPB within various radius values may cause alterations in the amount of gas–liquid interfacial effective surface area and MT rate. On the other hand, changes in the flow area in RPBs, contrary to that in PBCs, is significant when the MT coefficient varies with the position on the rotor because of gas velocity and surface area changes along the radius [28]. There are also significant parameters that can enhance the gas–liquid MT interfacial effective surface area. These parameters are summarized below according to the results of [73–76]:

1. Rotating speed, (affecting liquid elements);
2. Gas and liquid rate;
3. Packing form and configuration;
4. Liquid distribution;
5. Temperature.

The simplest technique that is used in chemical methods to calculate the amount of a_e is has been applied by numerous investigators using CO_2-NaOH or CO_2-N_2-NaOH

systems. For calculations, it is assumed that steady-state isothermal physical absorption occurs through the packing of an RPB and gas feed, assuming ideal gas.

In this study, the diffusivity, density, and viscosity of pure water and NFs were calculated according to [77,78], and Table 2 illustrates the NP specifications. The mean centrifugal acceleration was calculated using the following equation [79]:

$$a_m = \left(\frac{R_o^2 + R_i^2}{2}\right)^{\frac{1}{2}} \left(\frac{2\pi N}{60}\right)^2 \quad (1)$$

In addition, the gravity ratio can be calculated by dividing a_m by the earth gravity [55].

Physical absorption of CO_2 by NFs is related to NP surface active sites where ions and H_2O molecules are adsorbed and released in solution. HCO_3^- ions that interact with polar groups on NPs are generated through the reaction of CO_2 with water as follows [21]:

$$CO_2 + H_2O \leftrightarrow H_2CO_3 \leftrightarrow H^+ + HCO_3^- \quad (2)$$

Data gathering from the RPB setup was carried out using acid–base titration, which is used to estimate the amount of absorbed CO_2 by NFs, and finally the experimental k_La was calculated by considering the following stoichiometric reactions for acid-base titration:

$$2NaOH + CO_2 \rightarrow Na_2CO_3 + H_2O \quad (3)$$

$$2NaOH + H_2SO_4 \rightarrow Na_2SO_4 + 2H_2O \quad (4)$$

A total of 15 mL of NaOH of 0.01 M was consumed for titration of 2 mL of the solvent sample with H_2SO_4 (0.0024 M). The CO_2 rate at the RPB inlet (from the regeneration section) and outlet was computed using Equation (5). Then, the overall volumetric MT coefficient in the RPB was calculated using Equation (6).

$$\dot{N}_{CO2} = \frac{0.5\left[\left(v_{NaOH}.M_{NaOH}\right) - \left(2v_{H_2SO_4}.M_{H_2SO_4}\right)\right]}{v_{NF} \times 0.001} \times Q_{NF} \quad (5)$$

$$k_L a = \frac{\dot{N}_{CO2}^{L,inlet} - \dot{N}_{CO2}^{L,outlet}}{\Delta C_{ln}} \quad (6)$$

$$\Delta C_{ln} = \frac{\Delta C_1 - \Delta C_2}{ln\left(\frac{\Delta C_1}{\Delta C_2}\right)} \quad (7)$$

$$\Delta C_1 = HE.P_{g,inlet} - C_{L,outlet} \quad (8)$$

$$\Delta C_2 = HE.P_{g,outlet} - C_{L,inlet} \quad (9)$$

$$C_L = \frac{\dot{N}_{CO2}^{L}}{Q_{NF}} \quad (10)$$

where C_L is the CO_2 concentration and HE is the Henry coefficient, which was taken from [77]. The MT intensification parameter, k_{eff}, which was described as a ratio of the MT coefficients by Saeedina et al. [80], can show that *NF*s are more effective than BFs.

$$k_{eff} = \frac{(k_L a)_{NF}}{(k_L a)_W} \quad (11)$$

After the above calculations, the density and viscosity of the NFs were estimated by the following equations [81]:

$$\mu_{NF} = (1 + 2.5\varphi)\mu_w \quad (12)$$

$$\rho_{NF} = \varphi\rho_p + (1 - \varphi)\rho_w \quad (13)$$

$$\varphi(vol\%) = \frac{(wt\%)}{(wt\%) + \frac{\rho_p}{\rho_{BF}}(100 - wt\%)} \quad (14)$$

The diffusivity values of water were calculated with Equation (15), which was proposed by Versteeg and Swaaij [77], and the values for the NFs were extracted from the findings of [78]. The NP Reynolds number (Re_{NF}) was determined by Equation (16) [64].

$$D_{CO2,w} = 2.35 \times 10^{-6} \exp\left(\frac{-2119}{T}\right) \quad (15)$$

$$Re_{NP} = \frac{2k_B T \rho_p}{\pi \mu_{NF}^2 d_{particle}} \quad (16)$$

3. Results and Discussion

In the setup of this work, the gravity ratio increased from 30.06 to 219.04 from the inner radius of the packing to the outer radius, and from 53.45 to 389.40 at the low and high rotating speeds of the rotor, respectively. Regarding this issue, it was necessary to survey the effect of the rotating speed on the MT volumetric coefficient. Figure 3 shows the values of k_La of pure water and various NFs versus the CO_2 content of the gas feed, which reveals how the concentration of NPs and kind of NPs affected the MT performance. It was also found that the MT coefficient of Al_2O_3 NF- 0.01 wt at high/low rotating speeds (Figure 3a) and TiO_2 NF-0.05 wt.% were the highest values (Figure 3b), and the Al_2O_3 and TiO_2 NFs' MT volumetric coefficient v alues were higher than those of the SiO_2 NF at a concentration of 0.1 wt.% (Figure 3c). Figure 3d demonstrates that an increase in the rotating speed of the RPB led to an increase in the k_La values. The figure indicates that there was a relationship between k_La and the rotor speed. It also reveals that higher rotor speeds improved a_w. Therefore, the a_e values change along the radius for solvents, as reported by Agarwal et al. [82], and are influenced by changes in the NF concentration, type of NF, and CO_2 content. This may be due to the microconvection ability of NPs and its dependency on concentration values. A higher amount of CO_2 content also makes for a higher driving force due to further concentration differences between the phases.

To evaluate the effect of Al_2O_3, TiO_2, and SiO_2 concentration on MT performance, concentrations of 0.05, 0.01, and 0.1 were selected and examined at a constant gas flow rate of 10 L/min with different CO_2 content values (10–50 vol.%) and various solvent flow rates, as shown in Figure 4a–d. The figure demonstrates that k_La was influenced by the kind of nanoparticle as well as nanofluid concentration and flow rate, but it was not changed by varying the CO_2 content. This figure also indicates that NFs had substantially higher MT performance than water, which may be due to the shuttle effect, as well as hydrodynamic and bubble breaking effects in NFs, which can increase the contact area and reduce the boundary layer's thickness, which, as discussed by Kim et al. [83], can intensify the diffusion of CO_2 molecules [84]. Furthermore, it was found that the concentration of 0.01 wt.% of the NF was more efficient than other concentrations of the suspension. This result confirms Krishnamurthy et al.'s and Kim et al.'s reports [71,85], which demonstrated that an increase in the concentration values of NPs intensifies the diffusion up to a certain value and then decreases. In addition, viscosity does not have a significant effect because of low concentrations, as reported by Samadi [25].

As Figures 3a and 4, reveal, the NF concentration of 0.01 wt.% was tested at different flow rates and a constant gas flow rate (10 L/min) with two CO_2 content values (50 and 10 vol.%) which also included Al_2O_3 NFs (II). The results of these tests are shown in Figure 5.

Figure 5a,b reveal that the TiO_2 and Al_2O_3 NFs (II) were more effective than other NFs and pure water. In addition, as can be seen, the Al_2O_3 (II) NF was more effective than the Al_2O_3 (I) NF, which may have been due to high turbulence that occurs at higher gas and liquid flow rates, and more importantly due to effective surface area values and the microconvection ability of NPs.

Considering the data shown in Figure 5 and using Equation (11), the MT intensification parameter at high rotating speeds was calculated for Al_2O_3 (II), Al_2O_3 (I), TiO_2, and SiO_2. The average amount of k_{eff} at the high speeds of the RPB were 1.99, 1.47, 1.82, and 1.77 for Al_2O_3 (II), Al_2O_3 (I), TiO_2, and SiO_2, respectively, and the maximum value reached 2.59 for Al_2O_3 (II), which may have been due to its nanoscale mixing abilities in liquid.

In addition, the results shown in Figures 3–5 indicate that the performance of metal-oxide NPs was better than that of SiO_2 NF, which could be related to the microconvection, diffusion, and surface-active site ability of NFs, which can adsorb ions. In addition, surface renewal rate or acidic, basic, or amphoteric properties of NF can change the concentrations of H_3O^+ and OH^- [20].

On the other hand, it can be claimed that the Al_2O_3(II) NF performance was better than that of Al_2O_3(I), which may be related to surface area, as indicated in Refs. [23,86]. Based on the study carried out by Ali et al. [87], who showed that a nanofluid's thermal conductivity coefficient increases with the size of the NPs, and considering the similarity between heat and mass transfer, it may be argued that the better performance of the Al_2O_3(II) NF was due to the increase in the NPs.

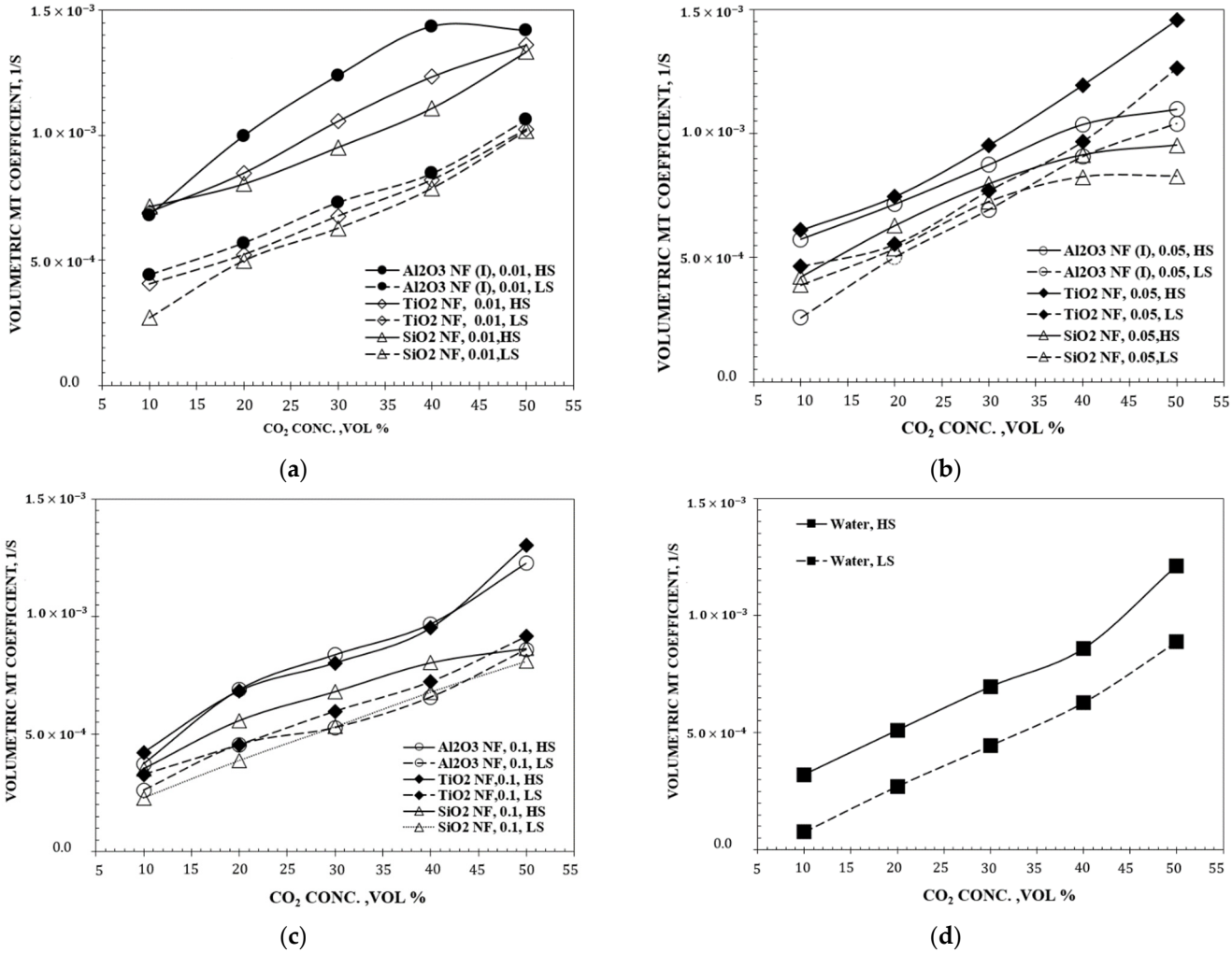

Figure 3. Volumetric MT coefficient (k_La) of NFs vs. CO_2 content at gas flow rate of 10 L/min, solvent flow rate of 30 L/h in high and low rotating speed. (**a**) 0.01 wt.% NFs, (**b**) 0.05 wt.% NFs, (**c**) 0.1 wt.% NFs and (**d**) pure water.

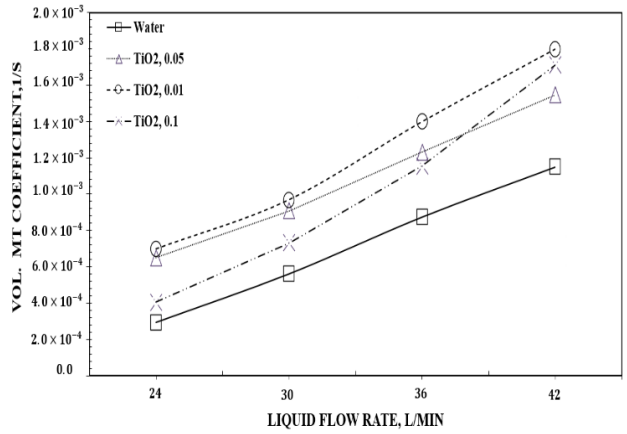

(**a1**) 50 vol.%

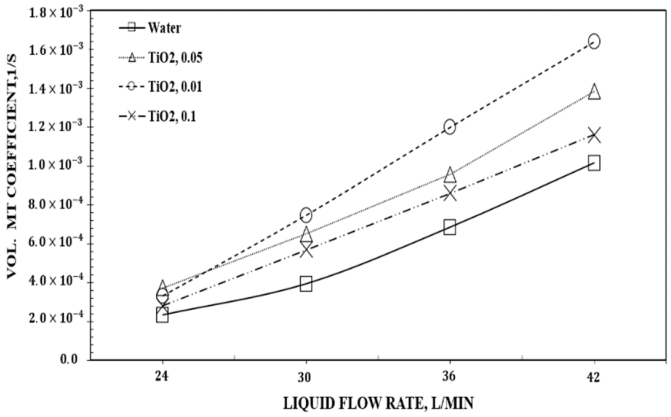

(**a2**) 25 vol.%

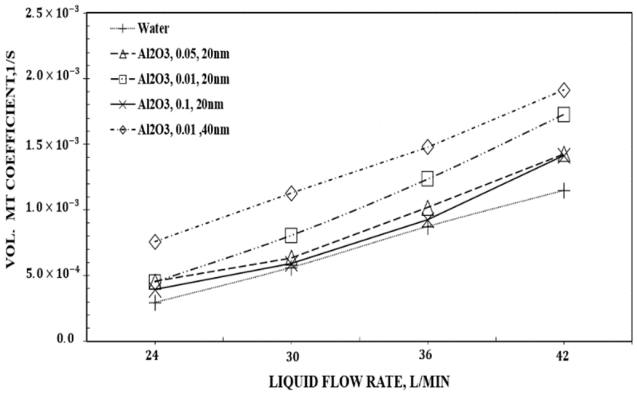

(**b1**) 50 vol.%

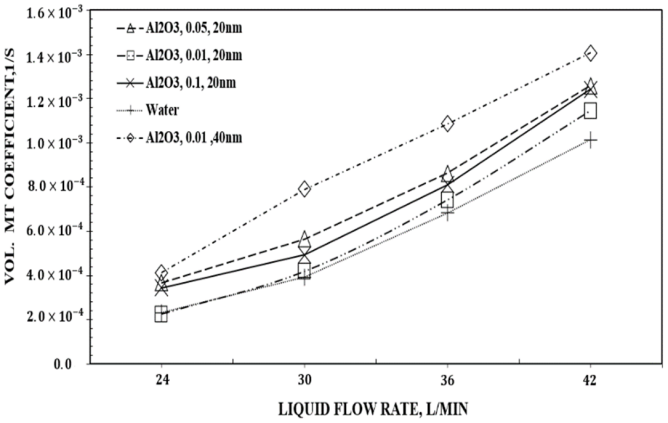

(**b2**) 25 vol.%

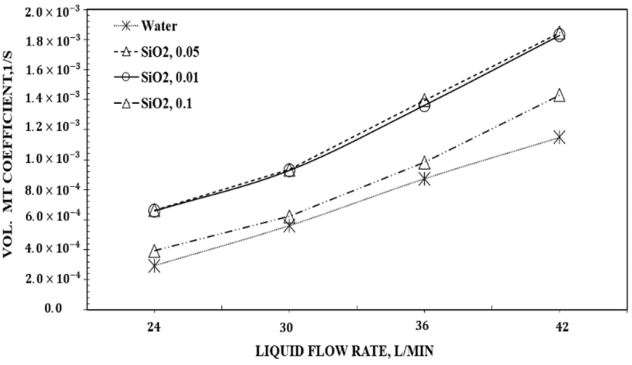

(**c1**) 50 vol.%

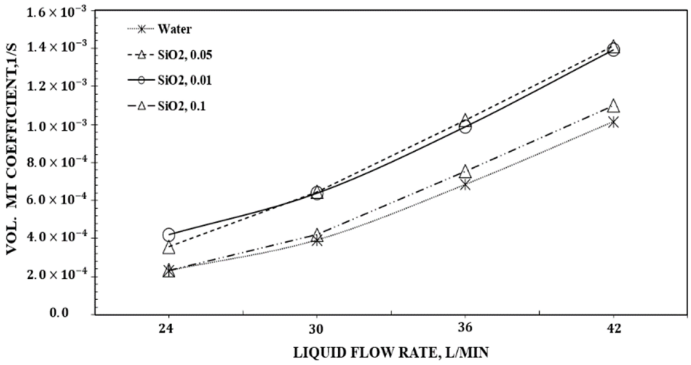

(**c2**) 25 vol.%

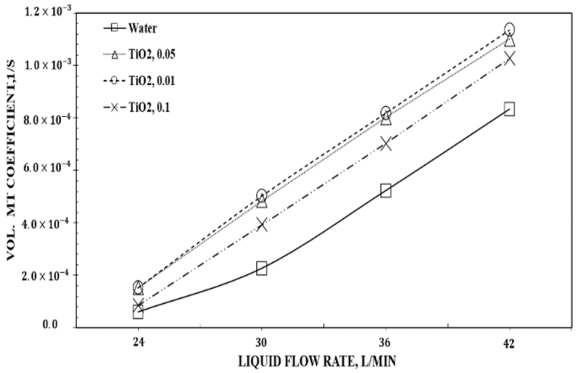

(**d1**) 10 vol.%

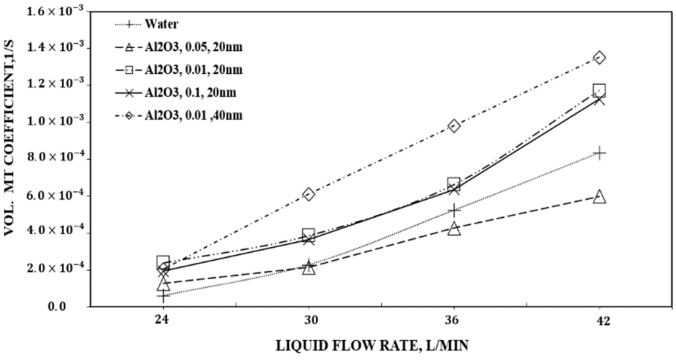

(**d2**) 10 vol.%

Figure 4. *Cont.*

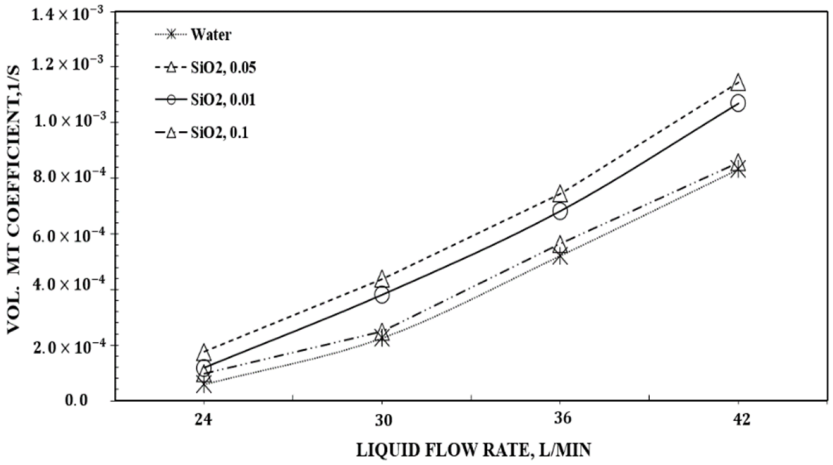

(**d3**) 10 vol.%

Figure 4. Volumetric MT coefficient ($K_L a$) of NFs (0.01, 0.05, and 0.1%wt) vs. flow rates at @ CO_2 50, 25 and 10 Vol.%, high rpm: 50 Vol. %. (**a1**,**b1**,**c1**), 25 Vol. %, (**a2**,**b2**,**c2**), 10 Vol. %, (**d1**,**d2**,**d3**).

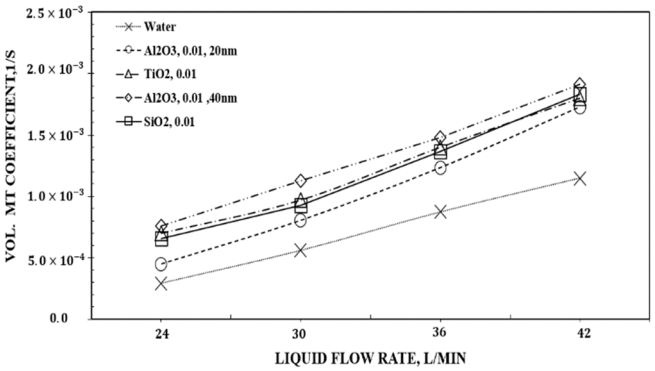

(**a**) 50 vol.%

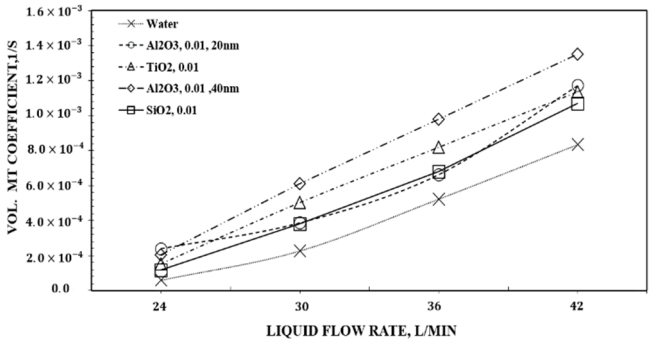

(**b**) 10 vol.%

Figure 5. $K_L a$ value comparison between NFs (0.01 wt.%) at gas flow rate of 10 L/min and high rotational speed vs. solvent flow rate at CO_2 content of (**a**) 50 vol.% and (**b**) 10 vol.%.

The effect of gas feed and solvent flow rates on the performance of Al_2O_3 (I) and (II) NFs-0.01 wt.% was examined (Figure 6). It is clear that the amount of $k_L a$ increased with an increase in the gas feed/solvent flow rate, and its values were higher at high rotating speeds than lower ones. Therefore, there was a relationship between the above-mentioned operating parameters and MT performance. Figure 6a shows the performance of Al_2O_3 (I) and (II) NFs (0.01 wt.%) at high rotating speeds, a constant CO_2 content of 50 vol.%, and two constant solvent flow rates of 24 and 42 L/h based on changes to the gas flow rate through the two upper solid curves along with the upper horizontal and right vertical axes, as well as the two lower dotted lines along with the lower horizontal and left vertical axes. Figure 6b similarly shows the performance of these two NFs at the same concentration, with a CO_2 content of 50 vol.% and at the constant gas flow rates of 6, 16, and 24 L/h based on changes to the solvent flow rate. It is also shown that sovereignty was related to Al_2O_3 (II). It is possible that the microconvection strength of Al_2O_3 (II) was higher than that of Al_2O_3 (I) in the solvent.

According to the flow regime, to predict the absorption performance of a contactor, it is necessary to determine the liquid-phase MT coefficient and Peclet Number (*Pe*) [72].

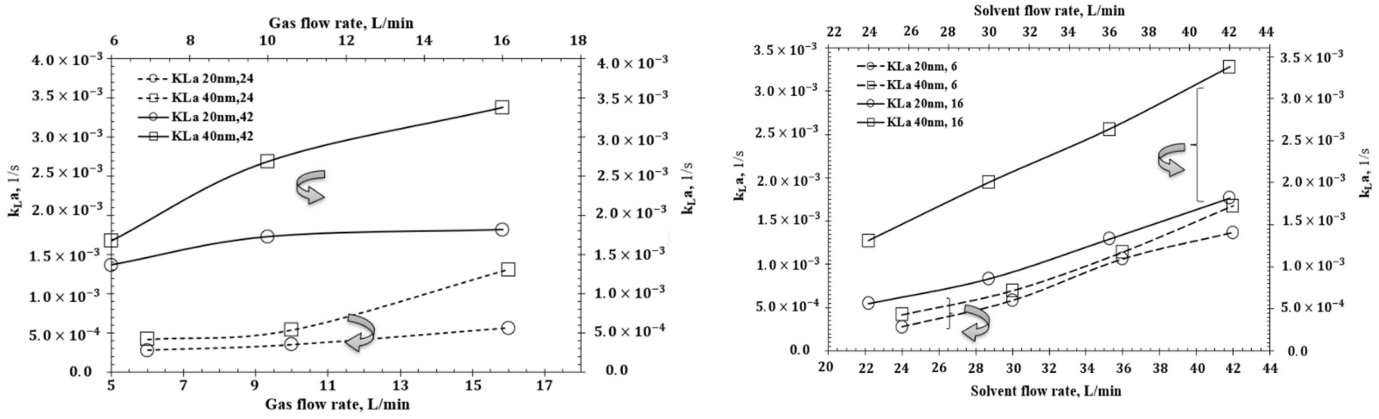

(**a**) (**b**)

Figure 6. Amount of $k_L a$ of Al_2O_3 NFs (0.01 wt.%) @ high rpm vs. (**a**) solvent flow rates of 24 and 42 L/h and (**b**) gas flow rates of 6 and 16 L/min.

Based on the MT correlations reported in [67], the above reported results, and evaluations of the correlations, it can be concluded that the volumetric MT coefficient was mostly proposed by investigators using Reynolds (*Re*), Schmidt (*Sc*), Weber (*We*), Froud (*Fr*), Grashof (*Gr*), and φ. For dimensional analysis, it is necessary to take into account parameters such as the geometry of the system, the process nature, kinematic viscosity, and external forces. Therefore, according to the above experimental results, the fact that external forces affect the turbulent situation of the fluid flow; the packing geometry; the liquid surface tension, which can be affected by the NP concentration and size; and the effect of rotational speeds considered with the *Re*, *Sc*, *We*, and *Gr* numbers should be all taken in to consideration. On the other hand, the relationship between $k_L a$ and the above-mentioned parameters can be expressed as follows:

$$k_L a = f\left(u_L,\ d_p, \rho_L, \mu_L, D_L, a_t, a_c, \sigma\right) \tag{17}$$

Taking into account the analogy of heat and mass transfer and considering the results of Kristiawan et al. [88] and Mohammadoost et al. [64], investigations in mass transfer have shown that when the absorbing solvent is an *NF*, the *NF*'s Reynolds number and concentration of *NF*s can affect the MT performance. Therefore, the above-mentioned issues, critical surface tension, and Brownian Reynolds number (Re_{NF}), which show the NP's role in micro-convention, lead to the following equation:

$$\frac{k_L a d_p}{D_L a_t} = A Re_G^a Re_L^b We_L^c Sc_L^d Gr_L^e \left(\frac{\sigma}{\sigma_c}\right)^f (B + \varphi Re_{NF})^g (B - \varphi Re_{NF})^h \tag{18}$$

In the present study, the constants of the empirical correlation of MT performance were found with regression analysis of the experimental data of water and *NF*s. This equation, known as the predicted model, showed a 29.7% discrepancy with the experimental data that were shown and compared with Rajan et al.'s [70] correlation (in Figure 7):

$$\frac{k_L a d_p}{D_L a_t} = 112.67 Re_G^{0.993} Re_L^{2.119} We_L^{0.331} Sc_L^{0.5} Gr_L^{0.294} \left(\frac{\sigma}{\sigma_c}\right)^{0.021} \left(\frac{1}{4} + \varphi Re_{NF}\right)^{3.543} \left(\frac{1}{4} - \varphi Re_{NF}\right)^{2.747} \tag{19}$$

The limitations of dimensionless numbers in the correlation were $5.29 \times 10^{-1} \leq Re_L < 9.26 \times 10^{-1}$, $1.55 \leq Re_G < 4.13$, $1.89 \times 10^{-6} \leq We \leq 7.68 \times 10^{-6}$, $6.66 \times 10^{1} \leq Sc \leq 3.18 \times 10^{-2}$, $4.12 \times 10^{5} + \leq Gr \leq 7.33 \times 10^{5}$, $0.00 \leq Re_{NP} \leq 1.31$.

$k_L a$ had higher Re_L and Re_{NP} power compared to other dimensionless groups, which shows that $k_L a$ was strongly connected to the liquid flow rate and NP concentration.

Considering the above-mentioned points about dimensionless groups, the above-mentioned relationship form can be used to scale up the RPB.

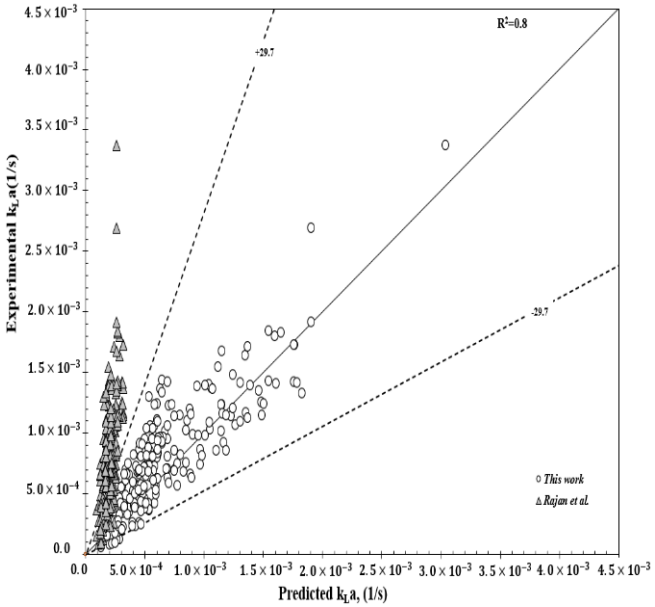

Figure 7. Experimental k_La vs. predicted k_La (Equation (18)) and Rajan et al.'s [70] correlation.

4. Conclusions

In this investigation, MT performance in a CO_2-N_2-NF system with centrifugal acceleration and several NPs was examined. The values of k_La for water, TiO_2, Al_2O_3, and SiO_2 NFs in various concentrations were obtained and the effect of changing operation parameters was analyzed. The metal oxides of TiO_2 and Al_2O_3 (I) and (II) were more efficient than the mineral oxide of SiO_2. Moreover, the concentrations of 0.01 wt.% were more efficient in comparison with the base fluid (water) and other concentrations of the suspension, and the NFs of TiO_2, Al_2O_3, and SiO_2 to some extent affected the liquid volumetric interfacial MT coefficient at the high rotating speeds of the RPB. The results clearly show that at high rpms, NPs in suitable concentrations can enhance the MT performance considerably, even when using low-solubility solvents like water at low pressure. In this study, Al_2O_3 (II) showed better performance and increased the amount of k_La approximately 2.6 times more than water.

Additionally, it can be pointed out that MT coefficients are a function of fluid properties and flow rates and change by variation of these quantities in the flow direction. A new correlation was also proposed (Equation (19)) in this study for k_La prediction at low pressure, which includes both the microconvection of NPs and the surface tension of packings. For future research on physical absorption, examining the process at higher system pressure and CO_2 concentration, adding extra intensification tools such as external magnetic forces, the use of the hybrid water-based NFs with Al_2O_3-TiO_2, a higher concentration of NPs and rpm, examination of MT interfacial effective surface area for NP participation, and more tests on other mineral NPs and advanced solvents such as biphasic, phase change, ionic liquids, and deep eutectic solvents are recommended.

Author Contributions: Data curation, F.G.; Investigation, F.G. and A.A.; Methodology, A.A. and A.V.; Project administration, A.A.; Software, F.G.; Supervision, A.A.; Validation, F.G.; Writing—original draft, F.G.; Writing—review & editing, A.A. and A.V. All authors have read and agreed to the published version of the manuscript.

Funding: This research received no external funding.

Data Availability Statement: The data presented in this study are available on request from the corresponding author.

Acknowledgments: We gratefully acknowledge the financial support of Bushehr Gas Company for this study.

Conflicts of Interest: The authors declare no conflict of interest.

Nomenclature and Greek Symbols

Nomenclature

a or a_e	Gas–liquid interfacial effective surface area per unit volume of bed, 1/m or m^2/m^3
a_c	Centrifugal acceleration, m/s^2, $a_c = r\omega^2$
a_p or a_t	Total packing surface area per unit volume of bed, 1/m
A	Gas–liquid MT interfacial area, m^2
$C_{L,inlet}$	CO_2 concentration at inlet stream of RPB, mol/m^3
$C_{L,outlet}$	CO_2 concentration at outlet stream of RPB, mol/m^3
$D_{CO2,\,w}$	Diffusivity of CO_2 in water, m^2/s
h	Ion constant (Na^+ = 0.091, OH^- = 0.066, $CO_3{}^{2-}$ = 0.021, and $h_G = -0.019$)
HE	Henry coefficient, mol/m^3 Pa
k_B	Boltzmann constant = 1.382×10^{-23} J/K
$K_G a$	Overall volumetric gas phase MT coefficient, 1/s
k_1	Pseudo-first-order reaction rate constant, 1/s
k_2	Pseudo-second-order reaction rate constant between CO_2 and OH^-, m^3/kmol s
$k_L a$	Local volumetric liquid phase MT coefficient, 1/s
$(k_L a)_{Exp.}$	Experimental value of liquid MT coefficient
$(k_L a)_{predic.}$	Predicted value of liquid MT coefficient by Equation (17)
m	Mass, kg
M_{NaOH}	Molarity of NaOH, mol/L
M_{H2SO4}	Molarity of H_2SO_4, mol/L
N	rpm (revolutions per minute)
N_{CO2}	CO_2 absorption flux, mol/m^2 s
N'_{CO2}	CO_2 absorption rate, mol/s
n	Number of data series
n'_{CO2}	Inlet molar flow rate of CO_2, mol/L
Q_G	Volumetric gas flow rate, m^3/s
Q_L	Volumetric liquid flow rate, m^3/s
R_i	Inner radius of packing, m
R_o	Outer radius of packing, m
R^2	Model's goodness of fit
Y_i	Inlet CO_2 concentration, %
Y_o	Outlet CO_2 concentration, %
Z	RPB packing height, m

Greek Symbols

ϕ	Pore diameter (mm) and volume fraction of NF (Equations (16) and (17))
ρ	Density, kg/m^3
μ	Dynamic viscosity
σ	Surface tension, kg/s^2 or N/m
σ_c	Critical surface tension of packing material, Kg/s^2 or N/m
γ	Contact angle, degree
ψ	Shape parameter of packing
ν	Kinematic viscosity, m^2/s
ν_{NaOH}	Consumed NaOH in titration, mL

Dimensionless Groups

$$Fr_L = \frac{Q_L^2}{a_c(2\pi rZ)^2 d_p}$$

$$Gr = \frac{a_c {d_p}^3}{\vartheta_L^2}$$

$$Re_L = \frac{Q_L d_p}{(2\pi rZ)v_L}$$

$$Re_G = \frac{Q_G d_p}{(2\pi rZ)v_G}$$

$$Re_{NP} = \frac{2K_B T \rho_{particle}}{\pi \mu^2 d_{particle}}$$

$$Sc_L = \frac{v_L}{D_L}$$

$$We_L = \frac{Q_L^2 d_p \rho_L}{(2\pi rZ)^2 \sigma}$$

Abbreviations

BF	Base fluid
DLS	Dynamic light scattering
DW	Distillated water
GLR	Gas–liquid ratio
MEA	Monoethanolamine
MT	Mass transfer
nm	Nanometer
NF	Nanofluid
NP	Nanoparticle

References

1. Merkel, T.C.; Lin, H.; Wei, X.; Baker, R. Power plant post-combustion carbon dioxide capture: An opportunity for membranes. *J. Memb. Sci.* **2010**, *359*, 126–139. [CrossRef]
2. Kenarsari, S.D.; Yang, D.; Jiang, G.; Zhang, S.; Wang, J.; Russell, A.G.; Wei, Q.; Fan, M. Review of recent advances in carbon dioxide separation and capture. *RSC Adv.* **2013**, *3*, 22739–22773. [CrossRef]
3. Tan, L.S.; Shariff, A.M.; Lau, K.K.; Bustam, M.A. Factors affecting CO_2 absorption efficiency in packed column: A review. *J. Ind. Eng. Chem.* **2012**, *18*, 1874–1883. [CrossRef]
4. Budzianowski, W.M. (Ed.) *Energy Efficient Solvents for CO_2 Capture by Gas-Liquid Absorption: Compounds, Blends and Advanced Solvent Systems*, 1st ed.; Springer: Berlin/Heidelberg, Germany, 2017. [CrossRef]
5. Li, B.; Duan, Y.; Luebke, D.; Morreale, B. Advances in CO_2 capture technology: A patent review. *Appl. Energy* **2013**, *102*, 1439–1447. [CrossRef]
6. Song, C.; Liu, Q.; Ji, N.; Deng, S.; Zhao, J.; Li, Y.; Song, Y.; Li, H. Alternative pathways for efficient CO_2 capture by hybrid processes—A review. *Renew. Sustain. Energy Rev.* **2017**, *82*, 215–231. [CrossRef]
7. Tong, D.; Maitland, G.C.; Trusler, M.J.P.; Fennell, P.S. Solubility of carbon dioxide in aqueous blends of 2-amino-2-methyl-1-propanol and piperazine. *Chem. Eng. Sci.* **2013**, *101*, 851–864. [CrossRef]
8. Liao, H.; Gao, H.; Xu, B.; Liang, Z. Mass transfer performance studies of aqueous blended DEEA-MEA solution using orthogonal array design in a packed column. *Sep. Purif. Technol.* **2017**, *183*, 117–126. [CrossRef]
9. Reay, D.; Ramshaw, C.; Harvey, A. *Process Intensification: Engineering for Efficiency, Sustainability and Flexibility*, 2nd ed.; Elsevier: Amsterdam, The Netherlands, 2013. [CrossRef]
10. Feng, D.; Gao, J.; Zhang, Y.; Li, H.; Du, Q.; Wu, S. Mass transfer in ammonia-based CO_2 absorption in bubbling reactor under static magnetic field. *Chem. Eng. J.* **2018**, *338*, 450–456. [CrossRef]
11. Boodhoo, K.; Harvey, A. *Process Intensification for Green Chemistry: Engineering Solutions for Sustainable Chemical Processing*; Wiley Online Library: Hoboken, NJ, USA, 2013; p. 413. [CrossRef]
12. Yu, C.H.; Chen, M.T.; Chen, H.; Tan, C.S. Effects of process configurations for combination of rotating packed bed and packed bed on CO_2 capture. *Appl. Energy* **2016**, *175*, 269–276. [CrossRef]
13. Chamchan, N.; Chang, J.Y.; Hsu, H.C.; Kang, J.L.; Wong, D.S.H.; Jang, S.S.; Shen, J.F. Comparison of rotating packed bed and packed bed absorber in pilot plant and model simulation for CO_2 capture. *J. Taiwan Inst. Chem. Eng.* **2017**, *73*, 20–26. [CrossRef]
14. Stankiewicz, A.I.; Moulijn, J.A. Process intensification: Transforming chemical engineering. *Chem. Eng. Prog.* **2000**. Available online: https://www.aiche.org/sites/default/files/docs/news/010022_cep_stankiewicz.pdf (accessed on 20 April 2022).
15. Ashrafmansouri, S.S.; Esfahany, M.N. Mass transfer into/from nanofluid drops in a spray liquid-liquid extraction column. *AIChE J.* **2015**, *62*, 852–860. [CrossRef]
16. Zhang, N.; Zhang, X.; Pan, Z.; Zhang, Z. A brief review of enhanced CO_2 absorption by nanoparticles. *Int. J. Energy Clean Environ.* **2018**, *19*, 201–215. [CrossRef]
17. Pineda, I.T.; Lee, J.W.; Jung, I.; Kang, Y.T. CO_2 absorption enhancement by methanol-based Al_2O_3 and SiO_2 nanofluids in a tray column absorber. *Int. J. Refrig.* **2012**, *35*, 1402–1409. [CrossRef]

18. Lee, J.W.; Kang, Y.T. CO_2 absorption enhancement by Al_2O_3 nanoparticles in NaCl aqueous solution. *Energy* **2013**, *53*, 206–211. [CrossRef]
19. Jiang, J.; Zhao, B.; Zhuo, Y.; Wang, S. Experimental study of CO_2 absorption in aqueous MEA and MDEA solutions enhanced by nanoparticles. *Int. J. Greenh. Gas Control* **2014**, *29*, 135–141. [CrossRef]
20. Haghtalab, A.; Mohammadi, M.; Fakhroueian, Z. Absorption and solubility measurement of CO_2 in water-based ZnO and SiO_2 nanofluids. *Fluid Phase Equilibria* **2015**, *392*, 33–42. [CrossRef]
21. Lu, S.; Song, J.; Li, Y.; Xing, M.; He, Q. Improvement of CO_2 absorption using AL_2O_3 nanofluids in a stirred thermostatic reactor. *Can. J. Chem. Eng.* **2015**, *93*, 935–941. [CrossRef]
22. Rahmatmand, B.; Keshavarz, P.; Ayatollahi, S. Study of Absorption Enhancement of CO_2 by SiO_2, Al_2O_3, CNT, and Fe_3O_4 Nanoparticles in Water and Amine Solutions. *J. Chem. Eng. Data* **2016**, *61*, 1378–1387. [CrossRef]
23. Darvanjooghi, M.H.K.; Esfahany, M.N.; Esmaeili-Faraj, S.H. Investigation of the effects of nanoparticle size on CO_2 absorption by silica-water nanofluid. *Sep. Purif. Technol.* **2018**, *195*, 208–215. [CrossRef]
24. Salimi, J.; Salimi, F. CO_2 capture by water-based Al_2NO_3 and Al_2O_3-SiO_2 mixture nanofluids in an absorption packed column. *Rev. Mex. Ing. Quim.* **2016**, *15*, 185–192.
25. Samadi, Z.; Haghshenasfard, M.; Moheb, A. CO_2 absorption using nanofluids in a wetted-wall column with external magnetic field. *Chem. Eng. Technol.* **2014**, *37*, 462–470. [CrossRef]
26. Salimi, J.; Haghshenasfard, M.; Etemad, S.G. CO_2 absorption in nanofluids in a randomly packed column equipped with magnetic field. *Heat Mass Transf. Stoffuebertragung.* **2014**, *51*, 621–629. [CrossRef]
27. Komati, S.; Suresh, A.K. CO_2 absorption into amine solutions: A novel strategy for intensification based on the addition of ferrofluids. *J. Chem. Technol. Biotechnol.* **2008**, *83*, 1094–1100. [CrossRef]
28. Reddy, K.J.; Gupta, A.; Rao, D.P.; Rama, O.P. Process intensification in a HIGEE with split packing. *Ind. Eng. Chem. Res.* **2006**, *45*, 4270–4277. [CrossRef]
29. Wang, G.Q.; Xu, O.G.; Xu, Z.C.; Ji, J.B. New HIGEE-rotating zigzag bed and its mass transfer performance. *Ind. Eng. Chem. Res.* **2008**, *47*, 8840–8846. [CrossRef]
30. Luo, Y.; Luo, J.Z.; Yue, X.J.; Song, Y.J.; Chu, G.W.; Liu, Y.; Le, Y.; Chen, J.F. Feasibility studies of micromixing and mass-transfer in an ultrasonic assisted rotating packed bed reactor. *Chem. Eng. J.* **2018**, *331*, 510–516. [CrossRef]
31. Dashti, M.S.A.; Abolhasani, M. Intensification of CO_2 capture by monoethanolamine solution containing TiO_2 nanoparticles in a rotating packed bed. *Int. J. Greenh. Gas Control* **2019**, *94*, 102933. [CrossRef]
32. Xiang, L.; Wu, L.; Gao, L.; Chen, J.; Liu, Y.; Zhao, H. Pilot Scale Applied Research on CO_2 Removal of Natural Gas Using a Rotating Packed Bed with Propylene Carbonate. *Chem. Eng. Res. Des.* **2019**, *150*, 33–39. [CrossRef]
33. Wang, Y.; Dong, Y.; Zhang, L.; Chu, G.; Zou, H.; Sun, B.; Zeng, X. Carbon dioxide capture by non-aqueous blend in rotating packed bed reactor: Absorption and desorption investigation. *Sep. Purif. Technol.* **2021**, *269*, 118714. [CrossRef]
34. Liu, Y.Z.; Wu, W.; Liu, Y.; Li, B.B.; Luo, Y.; Chu, G.W.; Zou, H.K.; Chen, J.F. Desulfurization intensification by ionic liquid in a rotating packed bed. *Chem. Eng. Processing-Process Intensif.* **2019**, *148*, 107793. [CrossRef]
35. Hacking, J.A.; Delsing, N.F.E.J.; de Beer, M.M.; van der Schaaf, J. Improving liquid distribution in a rotating packed bed. *Chem. Eng. Processing-Process Intensif.* **2020**, *149*, 107861. [CrossRef]
36. Hacking, J.A.; de Beer, M.M.; van der Schaaf, J. Gas-liquid mass transfer in a rotating liquid redistributor. *Chem. Eng. Processing-Process Intensif.* **2021**, *163*, 108377. [CrossRef]
37. Wu, W.; Luo, Y.; Chu, G.W.; Su, M.J.; Cai, Y.; Zou, H.K.; Chen, J.F. Liquid flow behavior in a multiliquid-inlet rotating packed bed reactor with three-dimensional printed packing. *Chem. Eng. J.* **2019**, *386*, 121537. [CrossRef]
38. Zhang, W.; Xie, P.; Li, Y.; Teng, L.; Zhu, J. CFD analysis of the hydrodynamic characteristics in a rotating packed bed with multi-nozzles. *Chem. Eng. Processing-Process Intensif.* **2020**, *158*, 108107. [CrossRef]
39. Wang, Y.; Li, Y.B.; Su, M.J.; Chu, G.W.; Sun, B.C.; Luo, Y. Liquid droplet dispersion in a rotating packed bed: Experimental and numerical studies. *Chem. Eng. Sci.* **2021**, *240*, 116675. [CrossRef]
40. Yang, Y.; Xiang, Y.; Li, Y.; Chu, G.; Zou, H.; Arowo, M.; Chen, J. 3D CFD modelling and optimization of single-phase flow in rotating packed beds. *Can. J. Chem. Eng.* **2015**, *93*, 1138–1148. [CrossRef]
41. Liu, W.; Luo, Y.; Liu, Y.Z.; Chu, G.W. Scale-Up of a Rotating Packed Bed Reactor with a Mesh-Pin Rotor: (I) Hydrodynamic Studies. *Ind. Eng. Chem. Res.* **2020**, *59*, 5114–5123. [CrossRef]
42. Liu, W.; Luo, Y.; Li, Y.B.; Chu, G.W. Scale-Up of a Rotating Packed Bed Reactor with a Mesh-Pin Rotor: (II) Mass Transfer and Application. *Ind. Eng. Chem. Res.* **2020**, *59*, 5124–5132. [CrossRef]
43. Su, M.J.; Le, Y.; Chu, G.W.; Li, Y.B.; Zhang, L.L.; Luo, Y. Intensification of Droplet Dispersion by Using Multilayer Wire Mesh and Its Application in a Rotating Packed Bed. *Ind. Eng. Chem. Res.* **2020**, *59*, 3584–3592. [CrossRef]
44. Lu, Y.-Z.; Liu, W.; Xu, Y.-C.; Luo, Y.; Chu, G.-W.; Chen, J.-F. Initial liquid dispersion and mass transfer performance in a rotating packed bed. *Chem. Eng. Processing-Process Intensif.* **2019**, *140*, 136–141. [CrossRef]
45. Yuan, Z.-G.; Wang, Y.-X.; Liu, Y.-Z.; Wang, D.; Jiao, W.-Z.; Liang, P.-F. Research and development of advanced structured packing in a rotating packed bed. *Chinese J. Chem. Eng.* **2022**. [CrossRef]
46. Groß, K.; de Beer, M.; Dohrn, S.; Skiborowski, M. Scale-Up of the Radial Packing Length in Rotating Packed Beds for Deaeration Processes. *Ind. Eng. Chem. Res.* **2020**, *59*, 11042–11053. [CrossRef]
47. Yuan, S.; Liu, Z.; Liu, G. High-gravity deoxygenation of jet fuels using rotating packed bed. *Fuel* **2022**, *314*, 123080. [CrossRef]

48. Ng, Y.S.; Tan, Y.T.; Chua, A.S.M.; Hashim, M.A.; Gupta, B.S. Removal of nickel from water using rotating packed bed contactor: Parametric studies and mode of operations. *J. Water Process Eng.* **2020**, *36*, 101286. [CrossRef]
49. Liu, Z.; Esmaeili, A.; Zhang, H.; Wang, D.; Lu, Y.; Shao, L. Modeling and Experimental Studies on Carbon Dioxide Absorption with Sodium Hydroxide Solution in a Rotating Zigzag Bed. *Processes* **2022**, *10*, 614. [CrossRef]
50. Jiao, W.; Yang, P.; Qi, G.; Liu, Y. Selective absorption of H_2S with High CO_2 concentration in mixture in a rotating packed bed. *Chem. Eng. Processing-Process Intensif.* **2018**, *129*, 142–147. [CrossRef]
51. Liu, Y.; Luo, Y.; Chu, G.W.; Larachi, F.; Zou, H.K.; Chen, J.F. Liquid microflow inside the packing of a rotating packed bed reactor: Computational, observational and experimental studies. *Chem. Eng. J.* **2019**, *386*, 121134. [CrossRef]
52. Chen, W.C.; Fan, Y.W.; Zhang, L.L.; Sun, B.C.; Luo, Y.; Zou, H.K.; Chu, G.W.; Chen, J.F. Computational fluid dynamic simulation of gas-liquid flow in rotating packed bed: A review. *Chinese J. Chem. Eng.* **2021**, *41*, 85–108. [CrossRef]
53. Cai, Y.; Luo, Y.; Chu, G.W.; Wu, W.; Yu, X.; Sun, B.C.; Chen, J.F. NOx removal in a rotating packed bed: Oxidation and enhanced absorption process optimization. *Sep. Purif. Technol.* **2019**, *227*, 115682. [CrossRef]
54. Liu, L. VOC removal in rotating packed bed: ANN model vs empirical model. *Alexandria Eng. J.* **2021**, *61*, 4507–4517. [CrossRef]
55. Jiao, W.Z.; Liu, Y.Z.; Qi, G.S. Gas pressure drop and mass transfer characteristics in a cross-flow rotating packed bed with porous plate packing. *Ind. Eng. Chem. Res.* **2010**, *49*, 3732–3740. [CrossRef]
56. Xing, Y.Q.; Liu, Y.Z.; Cui, L.J. Experimental study on intensification absorption of carbon dioxide from simulation flue gas by high-gravity rotary packed bed. *Mod. Chem. Ind.* **2007**, 470–473. Available online: http://en.cnki.com.cn/Article_en/CJFDTOTAL-XDHG2007S2139.htm (accessed on 20 April 2022).
57. Lin, C.-C.; Chen, B.-C. Carbon Dioxide Absorption into NaOH Solution in a Cross-flow Rotating Packed Bed. *J. Ind. Eng. Chem.* **2007**, *13*, 1083–1090. Available online: https://www.cheric.org/PDF/JIEC/IE13/IE13-7-1083.pdf (accessed on 20 April 2022).
58. Yu, C.H.; Cheng, H.H.; Tan, C.S. CO_2 capture by alkanolamine solutions containing diethylenetriamine and piperazine in a rotating packed bed. *Int. J. Greenh. Gas Control* **2012**, *9*, 136–147. [CrossRef]
59. Kang, J.L.; Sun, K.; Wong, D.S.H.; Jang, S.S.; Tan, C.S. Modeling studies on absorption of CO_2 by monoethanolamine in rotating packed bed. *Int. J. Greenh. Gas Control* **2014**, *25*, 141–150. [CrossRef]
60. Gao, X.Y.; Liu, L.; Hu, M.L.; Xiang, Y.; Chu, G.W.; Zou, H.K.; Sun, B.C.; Chen, J.F. Numerical simulation for mass transfer characteristics of CO_2 capture in a rotating packed bed. *Chem. Eng. Processing-Process Intensif.* **2016**, *109*, 68–79. [CrossRef]
61. Wu, T.W.; Hung, Y.T.; Chen, M.T.; Tan, C.S. CO_2 capture from natural gas power plants by aqueous PZ/DETA in rotating packed bed. *Sep. Purif. Technol.* **2017**, *186*, 309–317. [CrossRef]
62. Sheng, M.; Xie, C.; Zeng, X.; Sun, B.; Zhang, L.; Chu, G.; Luo, Y.; Chen, J.F.; Zou, H. Intensification of CO_2 capture using aqueous diethylenetriamine (DETA) solution from simulated flue gas in a rotating packed bed. *Fuel* **2018**, *234*, 1518–1527. [CrossRef]
63. Zhao, B.; Tao, W.; Zhong, M.; Su, Y.; Cui, G. Process, performance and modeling of CO_2 capture by chemical absorption using high gravity: A review. *Renew. Sustain. Energy Rev.* **2016**, *65*, 44–56. [CrossRef]
64. Mohammaddoost, H.; Azari, A.; Ansarpour, M.; Osfouri, S. Experimental investigation of CO_2 removal from N_2 by metal oxide nanofluids in a hollow fiber membrane contactor. *Int. J. Greenh. Gas Control* **2018**, *69*, 60–71. [CrossRef]
65. Treybal, R.E. *Mass Transfer Oerations*, 3rd ed.; McGraw-Hill Book Company: Singapore, 1981. [CrossRef]
66. Munjal, S.; Dudukovć, M.P.; Ramachandran, P. Mass-transfer in rotating packed beds-I. Development of gas-liquid and liquid-solid mass-transfer correlations. *Chem. Eng. Sci.* **1989**, *44*, 2245–2256. [CrossRef]
67. Ghadyanlou, F.; Azari, A.; Vatani, A. A Review of Modeling Rotating Packed Beds and Improving Their Parameters: Gas–Liquid Contact. *Sustainability* **2021**, *13*, 8046. [CrossRef]
68. Chen, Y.S.; Lin, C.C.; Liu, H.S. Mass transfer in a rotating packed bed with various radii of the bed. *Ind. Eng. Chem. Res.* **2005**, *44*, 7868–7875. [CrossRef]
69. Chen, Y.S.; Lin, F.Y.; Lin, C.C.; der Tai, C.Y.; Liu, H.S. Packing characteristics for mass transfer in a rotating packed bed. *Ind. Eng. Chem. Res.* **2006**, *45*, 6846–6853. [CrossRef]
70. Rajan, S.; Kumar, M.; Ansari, M.J.; Rao, D.P.; Kaistha, N. Limiting gas liquid flows and mass transfer in a novel rotating packed bed (HiGee). *Ind. Eng. Chem. Res.* **2011**, *50*, 986–997. [CrossRef]
71. Kim, S.; Xu, R.; Lee, W.; Kang, Y.T. Mass transfer performance enhancement by nanoabsorbents during CO_2 absorption process. *Int. J. Heat Mass Transf.* **2019**, *137*, 1–11. [CrossRef]
72. Fukushima, S.; Kusaka, K. Liquid-phase volumetric and mass-transfer coefficient, and boundary of hydrodynamic flow region in packed column with cocurrent downward flow. *J. Chem. Eng. JAPAN* **1977**, *10*, 468–474. [CrossRef]
73. Yang, K.; Chu, G.; Zou, H.; Sun, B.; Shao, L.; Chen, J.F. Determination of the effective interfacial area in rotating packed bed. *Chem. Eng. J.* **2011**, *168*, 1377–1382. [CrossRef]
74. Guo, K.; Zhang, Z.; Luo, H.; Dang, J.; Qian, Z. An innovative approach of the effective mass transfer area in the rotating packed bed. *Ind. Eng. Chem. Res.* **2014**, *53*, 4052–4058. [CrossRef]
75. Tsai, C.Y.; Chen, Y.S. Effective interfacial area and liquid-side mass transfer coefficients in a rotating bed equipped with baffles. *Sep. Purif. Technol.* **2015**, *144*, 139–145. [CrossRef]
76. Chen, Q.Y.; Chu, G.W.; Luo, Y.; Sang, L.; Zhang, L.L.; Zou, H.K.; Chen, J.F. Polytetrafluoroethylene wire mesh packing in a rotating packed bed: Mass-Transfer studies. *Ind. Eng. Chem. Res.* **2016**, *55*, 11606–11613. [CrossRef]
77. Versteeg, G.F.; van Swaal, W.P.M. Solubility and Diffusivity of Acid Gases (CO_2, N_2O) in Aqueous Alkanolamine Solutions. *J. Chem. Eng. Data* **1988**, *33*, 29–34. [CrossRef]

78. Dehghan, P.; Azari, A.; Azin, R. Measurement and correlation for CO_2 mass diffusivity in various metal oxide nanofluids. *J. Environ. Chem. Eng.* **2019**, *8*, 103598. [CrossRef]
79. Ramshaw, C.; Mallinson, R.H. Mass Transfer Process. U.S. Patent US4283255A, 11 August 1981.
80. Saeednia, L.; Hashemipour, H.; Afzali, D. Study on Mass Transfer Enhancement in a Gas-Liquid System Using Nanomaterials. *Transp. Phenom. Nano Micro Scales* **2015**, *3*, 46–53. [CrossRef]
81. Karamian, S.; Mowla, D.; Esmaeilzadeh, F. The effiect of various nanofluids on absorption intensification of CO_2/SO_2 in a single-bubble column. *Processes* **2019**, *7*, 393. [CrossRef]
82. Agarwal, L.; Pavani, V.; Rao, D.P.; Kaistha, N. Process intensification in HiGee absorption and distillation: Design procedure and applications. *Ind. Eng. Chem. Res.* **2010**, *49*, 10046–10058. [CrossRef]
83. Kim, J.H.; Jung, C.W.; Kang, Y.T. Mass transfer enhancement during CO_2 absorption process in methanol/Al_2O_3 nanofluids. *Int. J. Heat Mass Transf.* **2014**, *76*, 484–491. [CrossRef]
84. Jeong, M.; Lee, J.W.; Lee, S.J.; Kang, Y.T. Mass transfer performance enhancement by nanoemulsion absorbents during CO_2 absorption process. *Int. J. Heat Mass Transf.* **2017**, *108*, 680–690. [CrossRef]
85. Krishnamurthy, S.; Bhattacharya, P.; Phelan, P.E.; Prasher, R.S. Enhanced mass transport in nanofluids. *Nano Lett.* **2006**, *6*, 419–423. [CrossRef]
86. Lee, J.W.; Kim, S.; Pineda, I.T.; Kang, Y.T. Review of nanoabsorbents for capture enhancement of CO_2 and its industrial applications with design criteria. *Renew. Sustain. Energy Rev.* **2020**, *138*, 110524. [CrossRef]
87. Ali, F.M.; Yunus, W.M.M.; Talib, Z.A. Study of the effect of particles size and volume fraction concentration on the thermal conductivity and thermal diffusivity of Al_2O_3 nanofluids. *Int. J. Phys. Sci.* **2013**, *8*, 1442–1457.
88. Kristiawan, B.; Rifa'i, A.I.; Enoki, K.; Wijayanta, A.T.; Miyazaki, T. Enhancing the thermal performance of TiO_2/water nanofluids flowing in a helical microfin tube. *Powder Technol.* **2020**, *376*, 254–262. [CrossRef]